

Binding of ACE-inhibitors to in vitro and patient-derived amyloid- β fibril models

Manikanthan Bhavaraju, Malachi Phillips, Deborah Bowman, Juan M. Aceves-Hernandez, and Ulrich H. E. Hansmann

Citation: [The Journal of Chemical Physics](#) **144**, 015101 (2016);

View online: <https://doi.org/10.1063/1.4938261>

View Table of Contents: <http://aip.scitation.org/toc/jcp/144/1>

Published by the [American Institute of Physics](#)

Articles you may be interested in

[Stability of Iowa mutant and wild type A \$\beta\$ -peptide aggregates](#)

The Journal of Chemical Physics **141**, 175101 (2014); 10.1063/1.4900892

[Replica-exchange-with-tunneling for fast exploration of protein landscapes](#)

The Journal of Chemical Physics **143**, 224102 (2015); 10.1063/1.4936968



Binding of ACE-inhibitors to *in vitro* and patient-derived amyloid- β fibril models

Manikanthan Bhavaraju,¹ Malachi Phillips,¹ Deborah Bowman,² Juan M. Aceves-Hernandez,^{3,a)} and Ulrich H. E. Hansmann^{1,a)}

¹Department of Chemistry and Biochemistry, University of Oklahoma, Norman, Oklahoma 73019, USA

²Department of Biology, Langston University, Langston, Oklahoma 73050, USA

³Department of Chemistry, Facultad de Estudios Superiores Cuautitlán, Universidad Nacional Autónoma de México, Cuautitlán Izcalli, Estado de México, 15740, Mexico

(Received 3 September 2015; accepted 18 November 2015; published online 4 January 2016)

Currently, no drugs exist that can prevent or reverse Alzheimer's disease, a neurodegenerative disease associated with the presence, in the brain, of plaques that are composed of β -amyloid ($A\beta$) peptides. Recent studies suggest that angiotensin-converting enzyme (ACE) inhibitors, a set of drugs used to treat hypertension, may inhibit amyloid formation *in vitro*. In the present study, we investigate through computer simulations the binding of ACE inhibitors to patient-derived $A\beta$ fibrils and contrast it with that of ACE inhibitors binding to *in vitro* generated fibrils. The binding affinities of the ACE inhibitors are compared with that of Congo red, a dye that is used to identify amyloid structures and that is known to be a weak inhibitor of $A\beta$ aggregation. We find that ACE inhibitors have a lower binding affinity to the patient-derived fibrils than to *in vitro* generated ones. For patient-derived fibrils, their binding affinities are even lower than that of Congo red. Our observations raise doubts on the hypothesis that these drugs inhibit fibril formation in Alzheimer patients by interacting directly with the amyloids. © 2016 AIP Publishing LLC. [<http://dx.doi.org/10.1063/1.4938261>]

INTRODUCTION

Alzheimer's disease is the most common type of age-associated dementia and connected to the presence of plaques in the extracellular part of the brain. The plaques are made out of β -amyloid ($A\beta$) peptides which are of about 40–42 residues in length ($A\beta_{1-40}$ or $A\beta_{1-42}$).^{1,2} The neurotoxic entities, however, seems to be not the fibrils themselves but soluble oligomers that may be off-pathway to fibril-formation. Various *in vitro* studies have shown that the $A\beta$ oligomers are polymorphic and that their structures depend on the method of preparation and purification. For example, the Tycko group has determined different $A\beta$ fibril structures using solid-state NMR: one fibril model has two-fold symmetry (PDB ID: 2LMO)³ while a second one exhibits a three-fold symmetry (PDB ID: 2LMP).⁴ However, solid-state NMR data of fibrils acquired from a post mortem patient indicate that such polymorphism does not exist in the brains of Alzheimer's patients,⁵ as all samples contained only a single (patient-specific) structure characterized by a three-fold symmetry (PDB ID: 2M4J).⁵ The form of this patient-specific structure is correlated with the aggressiveness of the disease in the patient.⁵ All three fibril structures are shown in Figure 1 and have been studied by us in a previous study, where we found evidence that the lack of polymorphism in the patient-derived β -amyloid fibrils is not due to the higher stability of that structure.^{6–8}

In the present paper, we are interested in how the differences between the patient-derived structure and the

in vitro structures modulate the binding to potential drug candidates that may slow down, or reverse, Alzheimer's disease. This is an important question as current $A\beta$ inhibitors are developed using only *in vitro* $A\beta$ fibril structures.^{9,10} Hence, differences in binding to *in vitro* and patient-derived structures may explain the limited success of such drug candidates: presently, there are few effective FDA approved drug treatments for Alzheimer's disease and those that do exist, such as memantine and the four cholinesterase inhibitors donepezil, reminyl, razadyne, and rivastigmine, are poorly understood on a molecular level.^{11–14}

This is despite the many successful studies, both experimentally and computationally, that have investigated the interaction of small molecules with $A\beta$ monomers or fibril fragments, see, for instance,^{15,16} and the role of molecules such as polyphenols, carosine, Congo red (CR), thioflavin T as potential drug candidates.^{13,17–20} Polyphenol compounds such as curcumin,^{21,22} resveratrol,²³ ϵ -viniferin glucoside,²⁴ or epigallatechin gallate,²⁵ or small drug-like polypeptides^{26–28} have shown to inhibit effectively $A\beta$ aggregation, and some of them are now under phases II and III clinical trials.

Recently, it has been reported that the hypertensive drugs may also be helpful in treating Alzheimer disease.^{29–31} For example, consider the angiotensin converting enzyme (ACE) inhibitors, a class of drugs that for a long time has been used to treat hypertension³² but also seems to be correlated with reduced risk and severity of Alzheimer's disease in patients.^{33,34} The extensive knowledge on side-effects and contradictions of ACE inhibitors such as captopril, fosinopril, lisinopril, perindopril, ramipril, and trandolapril, and their ability to cross the blood-brain barrier, makes these compounds desirable drug candidates for the treatment of

^{a)}Authors to whom correspondence should be addressed. Electronic addresses: juanmanuel.is.aceves@gmail.com and uhansmann@ou.edu.

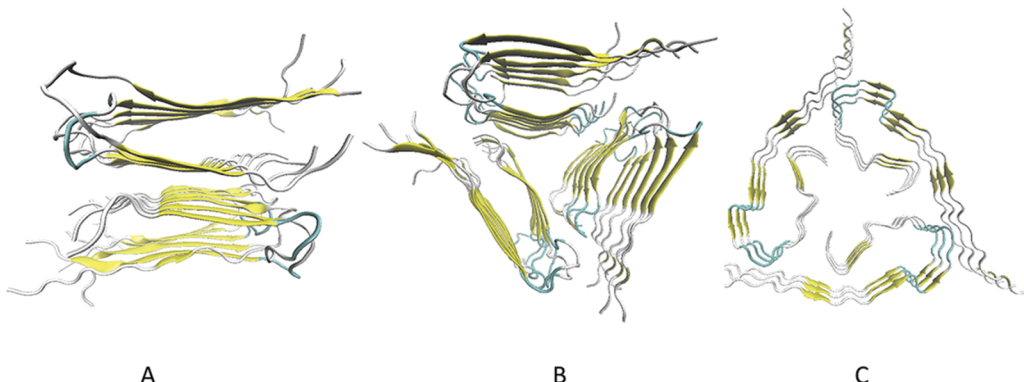


FIG. 1. Polymorphism in A β fibrils (a) is an *in vitro* fibril with two-fold symmetry (PDB ID: 2LMO), (b) is an *in vitro* fibril with three-fold symmetry (PDB ID: 2LMP), and (c) is the patient-derived fibril (PDB ID: 2M4J) which has a three-fold symmetry.

Alzheimer disease.³⁵ However, very little is known about the interaction of ACE inhibitors with the amyloid fibrils at the molecular level, i.e., whether these components inhibit amyloid formation or influence the pathology of Alzheimer's disease by another mechanism.

In order to test the possibility that these components influence directly amyloid formation, we investigate in this article the binding efficiency of various ACE inhibitors to three-fold six-layer models, build from either *in vitro* (2LMP) or patient-derived (2M4J) fibril structures, and we identify and compare potential binding sites. As a reference ligand, we choose Congo red, an amyloid staining agent and a weak inhibitor to amyloid formation.³⁶ Both structures consist of three β -sheets (β -sheets 1, 2, and 3) wherein each sheet contains six β -strands and has a hydrophobic central pore. This pore can act as water channel, potentially allowing for water leakage when inserted in the cell membrane, which may explain the toxicity of the amyloids.

While most computational studies have probed the interaction of small molecules with the two-fold A β fibril models, their interaction with three-fold models has also been researched. For instance, Li *et al.* did not only investigate with docking studies and explicit solvent molecular dynamics simulations of the binding of curcumin, ibuprofen, and naproxen, and β -sheet breaker peptides (KLVFF and LPFFD) to two-fold A β fibril models^{37,38} but also, using docking studies, proposed possible binding modes and interaction of these small molecules to three-fold three or six-layer *in vitro* A β fibril structures. One of their results is a correlation between binding energies of these components bound to the amyloids and aggregation inhibition efficiency. In the present paper, we assume as an initial hypothesis the same correlation, i.e., the stronger a component binds to the fibril structure the larger is its inhibition efficiency. New is not only the choice of ACE inhibitors as molecules that are studied but also that we compare their binding to *in vitro* form with the more physiologically relevant, and from a medical point of view more important, patient-derived fibril structure. To our knowledge, the interaction of the existing or newly proposed novel ligands with the most relevant patient-derived A β fibril structure has not been explored so far.

In most docking programs, the protein is treated as rigid, or only a specific loop or region is considered flexible. Only the

ligand is made flexible and is allowed to rotate or move. The binding modes are determined with search techniques such as random search,³⁹ Monte Carlo,⁴⁰ or genetic algorithms,⁴¹ using simple energy functions and an implicit solvent, to determine the binding affinity of a ligand to the protein. There are two problems with this approach. First, the protein structure needs to be an equilibrium structure. While one may assume that the ensemble of structures obtained by solvation NMR is a good approximation of the canonical ensemble at physiologically relevant temperatures, the situation is less clear in the case of solid-state NMR-derived structures. For this reason, we have chosen for our analysis not the first entry of the deposited NMR structures, but equilibrated fibril structures that were taken from our previous investigation and resulted from explicit solvent molecular dynamics runs of 300 ns duration.⁶ These equilibrated six-layer *in vitro* and patient-derived A β fibril structures are shown in Figure 2. A second problem in docking studies is that the energy functions do not take into account the behavior of the protein-ligand complex in an explicit solvent environment, i.e., do not account for solvent-solvent interactions and entropic effects, and since the protein is kept static and only the ligand is allowed to move, the estimated free energy differences ΔG values are not accurate. Hence, in order to obtain appropriate estimates of binding free energies for a protein-ligand system, one cannot simply rely on docking studies but has to calculate free energy differences from molecular dynamics simulations. While less accurate than free energy perturbation or thermodynamic integration, implicit methods such as the MM-GBSA (Molecular Mechanics - Generalized Born Surface Area) or MM-PBSA (Molecular Mechanics - Poisson-Boltzmann) approach have become widely used tools to rank the binding energies of a set of ligands with common structural features (such as ACE inhibitors).^{42,43} Again, such calculations require the presence of equilibrium configurations.

Analyzing the binding affinity of ten ACE inhibitors to equilibrated fibril structures, we find that these compounds bind more weakly to the patient-derived fibrils than to *in vitro* generated ones. While most of the ten ACE inhibitors bind more strongly to the *in vitro* generated fibril structure than Congo red, all of them bind less to patient-derived fibrils than Congo red. Our results therefore demonstrate the need to account for the polymorphism in A β -fibrils when designing drugs to inhibit fibril formation in Alzheimer patients.^{6,8,44,45}

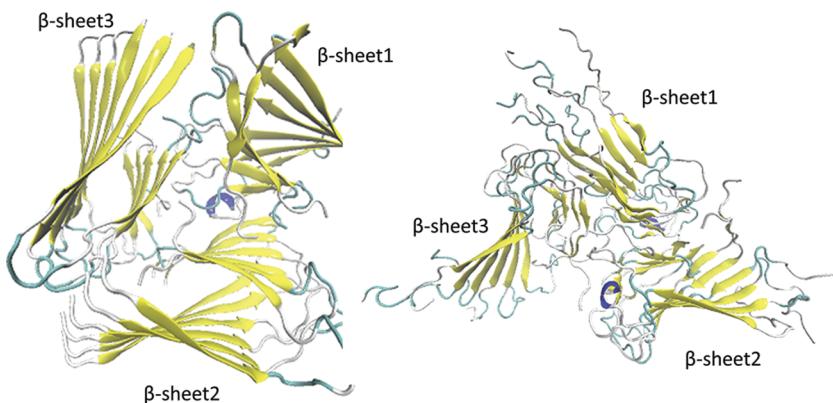


FIG. 2. Equilibrated *in vitro* (left) and patient-derived (right) three-fold six-layered $\text{A}\beta$ fibril structures.

COMPUTATIONAL METHODS

Docking studies

The structures of CR and of the ten studied ACE inhibitors are shown in Figure 3. All ligands are built using Spartan student version 5.0.1,⁴⁶ generating an ensemble of ligand configurations, with energies calculated by the MMFF94 method.⁴⁷ The lowest energy conformers are further optimized with HF/6-31G* using either Spartan or for the partial atomic charges of the ligands with the Restrained Electrostatic Potential (RESP) approach on the RESP ESP Derive online server.⁴⁸ The ligands are then individually docked to the equilibrated fibril models. As the predicted binding poses depend on the scoring functions and search algorithms implemented in given docking software, we decided to use in our study two distinct programs, namely, the Autodock Vina⁴⁹ and the Molegro⁵⁰ software. In the Molegro docking studies, we select for each system the lowest energy conformer as the best binding pose. In the case of Autodock Vina, for each system, the automatically generated nine lowest energy conformers are visually inspected using the VMD (Visual Molecular Dynamics) software.⁵¹ The conformers that bind to a specific binding pocket or β -sheet(s) are grouped together. For further analysis, we focus on the group with largest number of members and select its lowest energy conformer as the best binding pose. A similar kind of approach was applied in a previous study wherein the relative binding affinities of various ligands were in good agreement with the experimental observations.⁵² In order to check how our approach depends for Autodock Vina on the number of chosen conformers, we compared for each system the default of nine conformers with the case where 20 conformers were generated. We found that the Autodock Vina docking analysis performed using either with 9 or 20 conformers leads to similar best binding poses (see section titled Results and discussion). As altering the number of conformers seems to change little the best found binding pose, we choose for reason of simplicity the ones generated with the above protocol that start from the default number of conformers generated by Autodock Vina.

Molecular dynamics simulations

In order to investigate the binding of our ligands to the fibril models, we simulate the systems of solvated fibrils and ligands with explicit solvent model molecular dynamics.

 While the equilibrated fibril structures were originally generated in 300 ns-long molecular dynamics simulations⁶ that relied on the CHARMM27 force field with CMAP (cross term energy correction map) corrections,^{53,54} the simulations in this work are performed with the Amber12⁵⁵ software and rely on the ff12SB forcefield whose backbone and side chains torsion parameters are improved over that of the often used ff99SB.⁵⁶ This is because Amber's generalized atomic forcefield (*gaff*)⁵⁷ provides a simple mechanism for adapting the force field is adapted for ligands. We remark that we checked in preliminary test runs that our CHARMM-generated equilibrated fibril structures did not become unstable after switching force fields and are indeed equilibrium structures. Using *t leap*, the selected protein-ligand system is placed in the center of a cubic box and solvated with TIP3P⁵⁸ water molecules and an appropriate number of Na⁺ ions to neutralize the system. Because of periodic boundary conditions in our system, the electrostatic interactions are calculated by the Particle Mesh Ewald (PME)^{59,60} method using a 12 Å cutoff. The resulting system is first minimized over 20 000 steps with a constraint of 10 kcal mol⁻¹ Å⁻² on the protein, and afterwards for another 20 000 steps without any constraints. All systems are heated up to 298.15 K for 100 ps under NVT conditions, with a constraint of 10 kcal mol⁻¹ Å⁻² on the protein, and equilibrated for 1 ns under NPT conditions.

Each system is simulated twice for 50 ns under NVT conditions, with different initial velocities, resulting in two independent trajectories. During the equilibration and sampling, the hydrogens are constrained by the SHAKE algorithm,⁶¹ and Langevin dynamics⁶² with a collision frequency of 1.0 ps⁻¹ is used to keep the temperature constant. We use a time step of 2 fs.

The last 10 ns of the sampling process are used to calculate the binding free energies (ΔG_{GBSA}) in the MM-GBSA^{63,64} approximations, where the free energies are defined as

$$\Delta G = \Delta G_{\text{complex}} - \Delta G_{\text{receptor}} - \Delta G_{\text{ligand}}, \quad (1)$$

where $\Delta G_{\text{complex}}$ is the change in free energy of the protein-ligand complex, $\Delta G_{\text{receptor}}$ is the change in free energy of receptor, and ΔG_{ligand} is the change in free energy of ligand. In a MM-GBSA calculation the free energy differences are usually approximated by

$$\Delta G = \Delta E_{\text{forcefield}} + \Delta G_{\text{sol}} - T\Delta S, \quad (2)$$

where $\Delta E_{\text{forcefield}}$ is the gas phase internal energy of a system calculated using a pre-chosen forcefield, ΔG_{sol} is the change

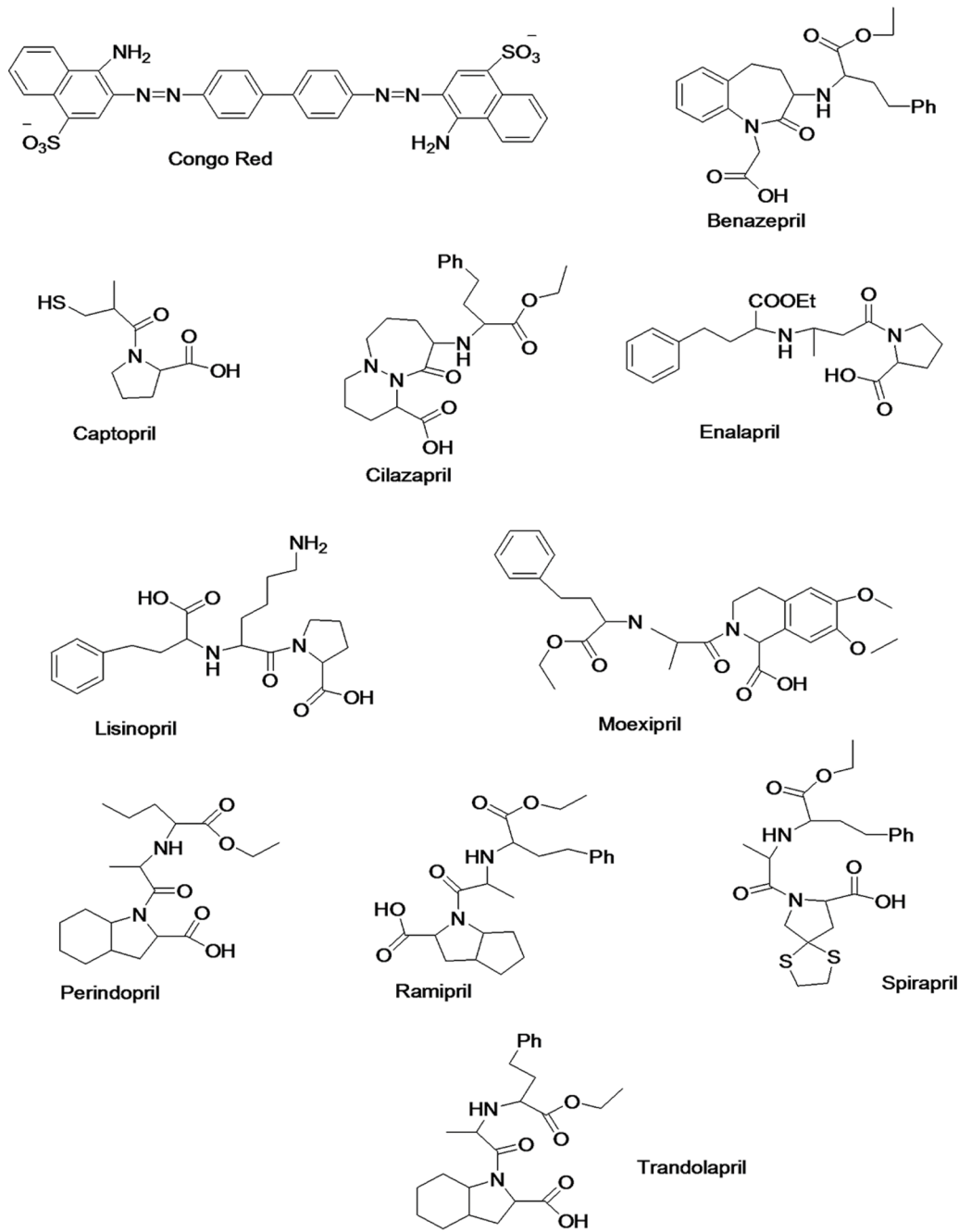


FIG. 3. Congo red and ten angiotensin converting enzyme inhibitors.

in the solvation free energy, and the entropy term $T\Delta S$ term is approximated in a normal mode analysis, which limits severely the estimation of entropy contributions by the MM-GBSA method.⁶⁵ The internal energy term consists of bonded terms (bond, angle, and torsion) and non-bonded terms (electrostatic (ΔE_{elec}) and van der Waals (ΔE_{vdw})) as shown below,

$$\Delta E_{forcefield} = \Delta E_{bonded} + \Delta E_{vdw} + \Delta E_{elec}. \quad (3)$$

Similarly, ΔG_{sol} consists of

$$\Delta G_{sol} = \Delta G_{elec} + \gamma SASA + b, \quad (4)$$

where ΔG_{elec} is an electrostatic term calculated using either a Poisson-Boltzmann or a generalized-Born (ΔG_{GB}) framework, SASA denotes the solvent accessible surface area, and γ and b are constants. While solving Poisson-Boltzmann equations

lead to a more accurate approximation of the electrostatic contributions, we use here generalized-Born approximation which is known to lead to similar binding energies but is computationally less expensive.^{42,66}

While the MM-GBSA method is more accurate than the even less costly empirical scoring, it is less accurate (but also less costly) than rigorous alchemical perturbation methods. Although its severe approximations limit the accuracy of the MM-GBSA method, it can be often used to reproduce and rationalize experimental findings. This is because the vibrational entropic contributions can be often neglected, for instance, if one, as in our case, is not interested in absolute values but in comparing the relative binding free energies of similar molecules. For this case, the entropy term is less important than when one considers absolute free energies, or

if significant conformational changes occur upon binding.^{67,68} As estimating the conformational entropy by normal mode analysis or quasi-harmonic approximation also often leads to large systematic and statistical errors, we exclude in this paper the conformational entropy term, a common approximation in amyloid studies.⁶⁹ However, we remark that while we believe that our use of MM-GBSA and our approximations are justified for our analysis of our systems, one has to be aware of their limitations. Especially, when interested in *absolute* values of the binding energies, one should use other, more accurate methods such as double-integration orthogonal space tempering technique.⁷⁰ Note also that we present in this study corrected MM-GBSA free energy values for the *in vivo* model that exclude contributions from the first eight residues. This is necessary to make our results comparable with the *in vitro* models where these residues are missing.

RESULTS AND DISCUSSION

Docking studies

We start our investigations of the binding of Congo red and ten ACE inhibitors to the *in vitro* and patient-derived 6-layer A β fibril models with docking studies comparing the Autodock Vina and Molegro docking software. Our goal is to contrast the binding patterns of the ACE inhibitors to the *in vitro* fibril structures with that of the inhibitors to the patient-derived fibril structures. The various binding patterns are compared with the corresponding binding patterns of Congo red interacting with the two fibril models. In Congo red, the biphenyl and naphthalene rings are linked together with N=N bonds which restricts rotations around these bonds. As a consequence, Congo red has to align in parallel or perpendicular orientation along the fibril axis when bound to A β fibril structure. On the other hand, the linker(s) which connects cyclic or aromatic rings of the chosen ACE inhibitors are connected through single bonds. The resulting higher flexibility (see Figure 3) may allow for more favorable binding modes.

In case of Autodock Vina, the ligands bind to various strands on all three β -sheets, or to the central column, of the *in vitro* fibril model. With the exception of enalapril and lisinopril, the binding location did not depend on whether we started our analysis initially with the default of nine conformers or with 20 conformers. On the other hand, the structures generated for enalapril and lisinopril when starting with 20 conformers resemble the ones found when using the Molegro software for docking. With this software, all ligands except benazepril and captopril bind to the central column. The binding positions for each ligand are tabulated in Table I. The ligands cilazapril, perindopril, ramipril, and trandolapril can bind to the central column with similar docking positions, but the orientation and interactions depend on the choice of docking program (Autodock Vina and Molegro) as shown in Figure 4. For instance, in the Molegro docking studies, perindopril interacts with various strands of β -sheet 3, whereas in Autodock Vina, perindopril interacts with strands of both β -sheets 2 and 3. The binding sites of the remaining seven ligands differ depending on the docking software. Irrespective of their binding positions, we label the selected conformers as

*in vitro*_{autodock} in the case of Autodock Vina and *in vitro*_{molegro} for the case of Molegro.

In case of the equilibrated patient-derived fibril structure, none of the ligands is bound to the central column as the shape and structure of the central column was lost over the 300 ns of the trajectory that led to this structure. The respective binding strand/pockets of the ligands as determined by Molegro or Autodock Vina are also listed in Table I. The listed values for Autodock Vina are again the ones obtained for the default of nine conformers as starting point of our analysis. When starting with 20 conformers, one finds best binding poses that are consistent with the ones in Table I, i.e., our results do not depend on the number of conformers initially generated by Autodock Vina.

Using Autodock Vina, many of the ligands interact with various strands of β -sheet 1, while interacting with β -sheet 3 in Molegro. As the binding locations depend again on the docking program, we label the ones found by Autodock Vina as (*PD*_{autodock}, where PD abbreviates patient-derived), and the ones found by Molegro as *PD*_{molegro}. Note that unlike for the *in vitro* model, we find no common binding pattern for the ligand that is independent of the docking software; instead, the binding sites and pockets differ for all ligands and depend on the software. The binding positions of the selected lower energy conformer of ligands binding to the equilibrium *in vitro* (*in vitro*_{autodock} and *in vitro*_{molegro}) and patient-derived A β fibril structures (*PD*_{autodock} and *PD*_{molegro}) are shown in Figure 5.

TABLE I. Binding sites of all ligands bound to equilibrated *in vitro* and patient-derived A β fibril models as derived by either Autodock Vina or Molegro docking software.

	Autodock Vina	Molegro
<i>In vitro</i> six-layer A β fibril		
Congo red	2 and 3	CC ^a
Benazepril	1 and 3	2 and 3
Captopril	1 and 3	2 and 3
Cilazapril	CC	CC
Enalapril	1 and 3	CC
Lisinopril	2	CC
Moexipril	2 and 3	CC
Perindopril	CC	CC
Ramipril	CC	CC
Spirapril	1 and 3	CC
Trandolapril	CC	CC
Patient-derived six-layer A β fibril		
Congo red	3	2 and 3
Benazepril	1 and 2	3
Captopril	1	3
Cilazapril	1	2
Enalapril	2	3
Lisinopril	2	2 and 3
Moexipril	1 and 2	1
Perindopril	1 and 2	3
Ramipril	1	3
Spirapril	1	2 and 3
Trandolapril	1	3

^aCC = central column.

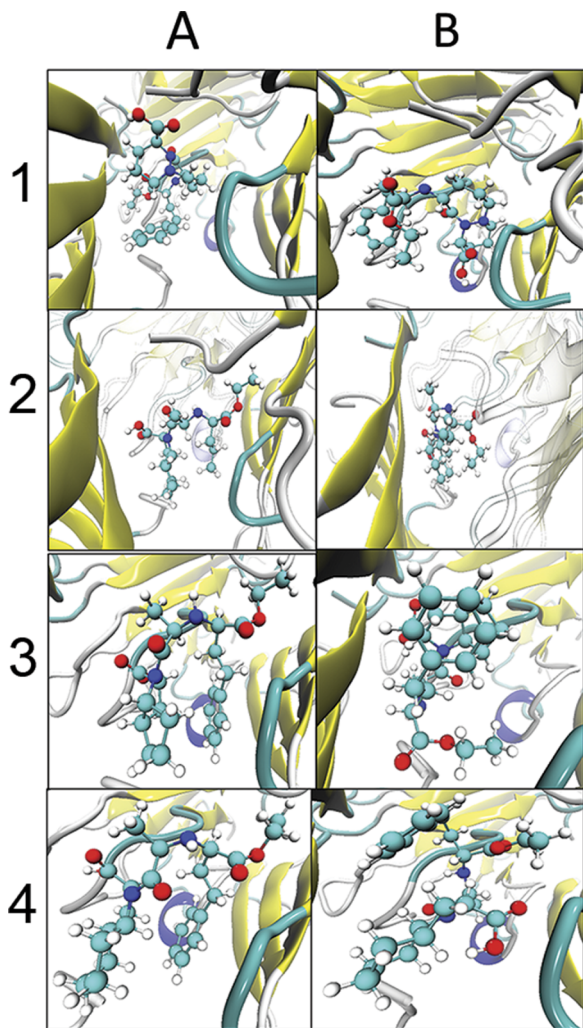


FIG. 4. Orientation of the selected lowest energy conformers of (1) cilazapril, (2) perindopril, (3) ramipril, and (4) trandolapril bound to an equilibrated *in vitro* fibril structure analyzed using Autodock Vina (a) and Molegro (b) docking software.

As the equilibrated patient derived structure is less compact than the first entry of the NMR ensemble (PDB-ID: 2M4J), we have compared our docking results of the equilibrated structure also with that of this structure and with the entry #20 of the NMR ensemble, which has with 9.5 Å the largest root-mean-square deviation (RMSD) to the first entry. Out of these two NMR structures (which have 3-layers), we have generated six-layer structures and minimized these to avoid steric clashes before using them in our docking studies. Using Autodock Vina, we find similar binding sites for the energy minimized structures as for the equilibrium structures, however, for the fibril generated from the first NMR entry all ligands except captopril can also bind to the central column. For this reason, we have also considered these binding modes in our binding free energy analysis and label the corresponding systems as PD_{First} .

Unlike for globular proteins, the $\text{A}\beta$ fibrils do not have well-defined binding or active sites as they contain β -sheets stacked on top of each other and arranged in various symmetry folds. This makes it difficult to assess the binding modes of the ligands to the $\text{A}\beta$ fibrils or oligomers that are found

with a docking program and used the poses generated by both Autodock Vina and Molegro. This is the reason why we compare in our docking studies two programs and use poses generated by both Autodock Vina and Molegro for our analysis. With both Autodock Vina and Molegro, we find as a common trend, independent of the software, that most ligands have more than a single binding pocket when docked to the *in vitro* or the patient-derived fibril model and that for all ligands the binding patterns differ between the two fibril models. None of the ligands binds to similar binding pockets in the *in vitro* model than seen for it in the patient-derived model. In order to understand these different binding patterns, it is necessary to determine their binding energies. Such an analysis requires the molecular dynamics simulations described in section titled Molecular dynamics simulations where we consider each of the eleven ligands bound to either the equilibrated *in vitro* or the patient-derived fibril model, taking as start configuration the best binding poses derived with either Molegro or Autodock Vina, i.e., a total of 44 ligand-protein systems. Note that the first eight residues are missing in the *in vitro* fibril models but are part of the patient derived structures. In order to compare the binding of the various ACE inhibitors to either *in vitro* or patient-derived structures, we have therefore excluded in the following analysis interaction of the ligands with the first eight residues.

Molecular dynamics simulations

Binding analysis of Congo red

All 44 systems are simulated in two independent trajectories (i.e., starting from the same configuration but different velocity distributions) for 50 ns with explicit solvent molecular dynamics simulations using Amber12 and the ff12SB force field. We start our analysis of these molecular dynamics runs by comparing the binding pattern of Congo red to both $\text{A}\beta$ fibrils with that found in previous computational/experimental studies.^{36,71,72} This allows us to validate the correctness of our simulation and analysis protocol.

Congo red is an amphiphilic and linear molecule whose long axis aligns parallel to the fibril axis when binding to amyloid fibrils in the grooves made of hydrophobic-aromatic N-terminal residues of the β -sheets. The two sulfate groups play a major role in driving the binding process.³⁶ Various binding orientations of the Congo red are observed, with the parallel orientation the most favorable one.

In our docking studies, the long axis of the Congo red is parallel to the fibril axis upon binding with the *in vitro* fibril structure at binding site $in vitro_{autodock}$ and with the patient-derived structure at binding site $PD_{autodock}$, i.e., in the two binding sites found with Autodock Vina. For the binding sites found by Molegro, $in vitro_{molegro}$ and $PD_{molegro}$, the ligand is perpendicular to the fibril growth. All four cases are shown in Figure 6. While the orientation of the ligand seems to depend on the docking software, the software does not lead to the same contacts for the two fibrils. In the case of the *in vitro* fibril structure $in vitro_{autodock}$, the molecule interacts with the

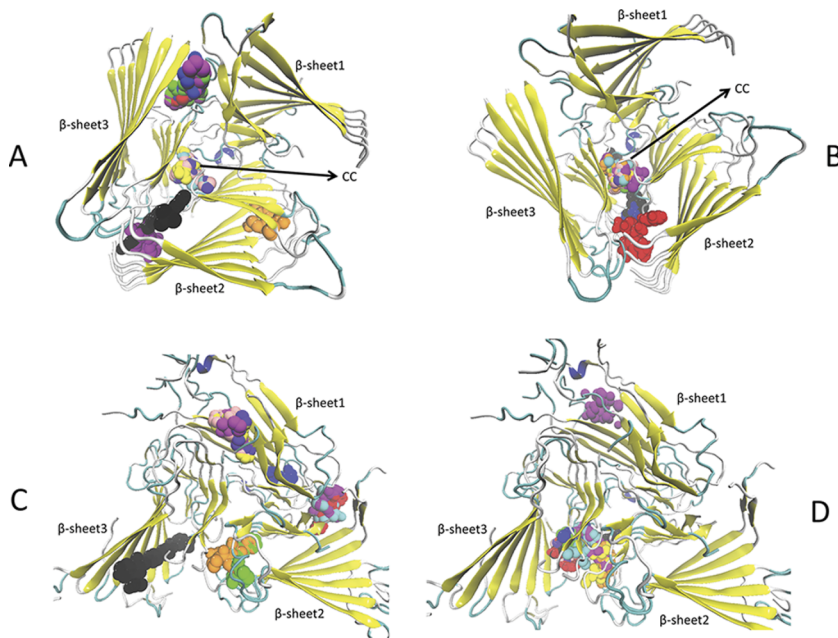


FIG. 5. Binding position of the lowest energy conformer of all the ligands when bound to the equilibrated *in vitro* and patient-derived A β fibrils as predicted by Autodock Vina and Molegro software, where (a) *in vitro* A β fibril-ligands Autodock Vina and (b) *in vitro* A β fibril-ligands Molegro docking analysis; (c) patient-derived A β fibril-ligands Autodock Vina and (d) patient-derived A β fibril-ligands Molegro docking analysis; Congo red = black, benazepril = red, captopril = blue, cilazapril = yellow, enalapril = green, lisinopril = orange, moexipril = purple, perindopril = cyan, ramipril = violet, spirapril = magenta, and trandolapril = pink.

residues Val12, His14, Lys28, and Gly29 located on various strands of the β -sheets 2 and 3. On the other hand, in the patient-derived fibril structure $PD_{autodock}$, Congo red resided in the groove formed by N-terminus residues His13 and Gln15 and interacts with His13, His14, and Gln15, all located on the 6-strands of β -sheet 3 as shown in Figure 7. Similarly, in the perpendicular alignment of $in vitro_{molegro}$, Congo red interacts with the hydrophobic residues (Gly4, Gly29, Ala30, Ile32, Val36, Gly38, Val39, and Val40) located in various strands of β -sheets 1, 2, and 3. When binding to the patient-derived structure in $PD_{molegro}$, the molecule interacts with the residues Gln15, Met35, and Val39 of various strands of β -sheets 2 and 3.

For the above discussed binding sites of Congo red, the average RMSD of the ligand, averaged MM-GBSA estimates of the binding energies (ΔG_{GBSA}), and average number of contacts between heavy atoms of the fibril structure and

the ligand are calculated over the last 10 ns of the two trajectories. The averaged values are tabulated in Table II. Here, we define a contact by the condition that two atoms are closer than 5 Å. Free energy differences, average RMSD and average number of contacts between fibril and ligand differ little in the case of Congo-red bound to the equilibrated *in vitro* fibril. The differences between the sites predicted by Molegro or Autodock Vina are larger in the case of the patient-derived structure, but binding sites generated by both programs have lower free energies and a larger number of contacts than seen for Congo red binding to the *in vitro* structure. For our comparison with the ACE inhibitors, we choose the complexes with the lowest free energy, i.e., $in vitro_{molegro}$ for binding of Congo red to the equilibrated *in vitro* fibril structure, and $PD_{autodock}$ for binding of Congo red to the equilibrated patient-derived fibril structure.

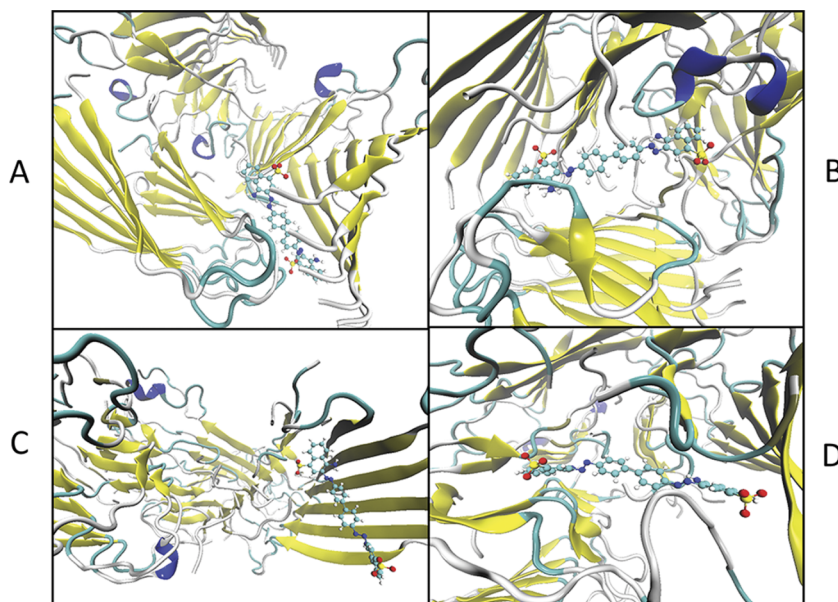


FIG. 6. Congo red bound to equilibrated *in vitro* and patient-derived A β fibril models, with (a) *in vitro* A β fibril-Congo red in parallel orientation at *in vitro*_{autodock}, (b) *in vitro* A β fibril-Congo red in perpendicular orientation at *in vitro*_{molegro}, (c) patient-derived A β fibril-Congo red in parallel orientation at $PD_{autodock}$, and (d) *in vitro* A β fibril-Congo red in perpendicular orientation at $PD_{molegro}$ binding sites.

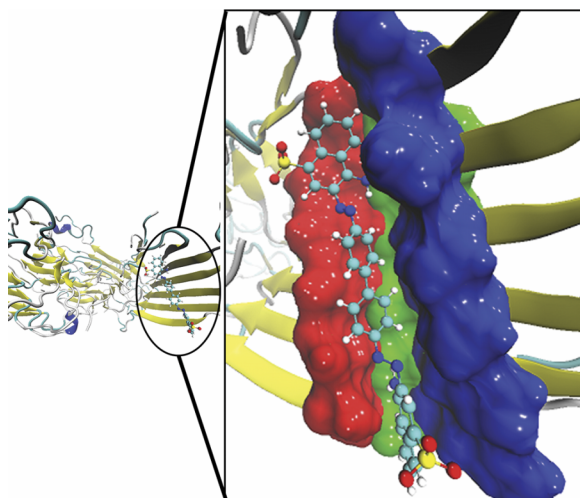


FIG. 7. Interaction of Congo red with Gln13, His14, and His15 of the six strands of β -sheet 3 when bound to patient-derived fibril at binding site $PD_{autodock}$ where blue = Gln13, green = His14, and red = His15.

Binding analysis of angiotensin converting enzyme inhibitors

Similar to the Congo red study, complexes of the various ACE inhibitors bound to either *in vitro* or patient-derived fibrils are followed over two independent molecular dynamics trajectories of 50 ns each. We use again only the last 10 ns for our analysis. The average RMSDs of the ACE inhibitors bound to *in vitro*/patient-derived fibril models are similar for both fibrils, and no significant difference is seen between binding sites derived from Autodock Vina or Molegro (data not shown).

In order to obtain a more detailed picture we have identified the residues that are involved in hydrogen bonding or hydrophobic interactions. For instance, the residues which exhibited these interactions with cilazapril and moexipril bound to *in vitro* fibril are shown in Figure 8(a) and that of lisinopril bound to the patient-derived structure shown in 8(b). We further display in Fig. 9 the average probability of residues in either the patient-derived or *in vitro* fibril models to form hydrophobic contacts with an ACE inhibitor. We see that the residues 27–40 (such as Asn27, Lys28, Ile31, Met35, Val39) are likely to form hydrophobic contacts with the ACE inhibitors upon binding to the *in vitro* structure, while the probability distribution is widely spread across all

the residues 1–40 when bound to patient-derived structure. We remark that the ACE inhibitors form mainly contacts with the main chain atoms of the *in vitro* fibril structure while they prefer to form contacts with the side chain atoms of the patient-derived structure. The above pattern in the probability distribution of contacts can be also seen in Table III where we list the residues involved in hydrogen bonding with the ACE inhibitors. In the majority of cases, hydrogen bonding is with the carboxylic group of the ACE inhibitors. Hydrogen bonding is mostly with C-terminus residues of the *in vitro* structure; however, no common trend is observed for the patient-derived fibril. Hence, the ACE inhibitors prefer to interact with the C-terminus residues of the *in vitro* fibril by hydrogen bonding and hydrophobic interactions. However, no such defined binding region can be designated to the ACE inhibitors when bound to patient-derived structure. This implies that all the ACE inhibitors have similar binding mode to the *in vitro* $\text{A}\beta$ fibril and different or independent binding poses interacting with the patient-derived structure.

In order to compare the binding efficiency of various ACE inhibitors with respect to Congo red, we have calculated the binding free energies of the ligands bound to either the *in vitro* or the patient derived fibril models with the MM-GBSA method for all binding sites. Again, the ΔG_{GBSA} values calculated using the last 10 ns of the two trajectories. For all *in vitro*/patient-derived fibril-ACE-inhibitor complexes are the binding free energy values averaged over both trajectories and tabulated in Table IV. For all our systems, we have also calculated the number of contacts between ACE inhibitors and *in vitro* or patient-derived fibril using the last 10 ns of the trajectories. The averages over the two trajectories are tabulated in Table V.

As a rule, the average binding free energies are lower for the ACE inhibitors bound to the equilibrated *in vitro* fibril structure than for the molecules bound to the equilibrated patient-derived fibril. This is likely due to the larger pore diameter in the patient derived fibrils. In the *in vitro* fibril structure the residues in the central tunnel are tightly packed and are held together due to strong hydrophobic interactions. When the ligand enters into the narrow pore region, it interacts with the mostly hydrophobic residues 27–40 and gets strongly bound to the central tunnel. On the other hand, the larger available space within the inner pore of the patient derived fibril. The net effect is that the ligands have weaker binding affinities with the residues 27–40 in the patient-derived fibril than in the *in vitro* structure. In the case of the *in vitro* systems, the free energy values of the binding sites generated by Molegro and the Autodock Vina are correlated (the R^2 value was 0.62), while no such correlation is found for the binding sites at the equilibrated patient-derived fibril. With the exception of captopril, the values differ little for the *in vitro* bound ACE inhibitors. Captopril is the smallest of the ten ACE inhibitors and has within this group the lowest number of interaction sites or groups that can participate in hydrogen bonding, van der Waals, electrostatic, or π - π stacking with the various residues of the patient-derived fibril (see Figure 3). As a consequence, captopril interacts only with Glu11 (strand 6 of β -sheet 3) when bound to the *in vitro* fibril structure, while the other ligands interact with multiple residues on various strands

TABLE II. Average root mean square deviation (RMSD) of Congo red, average number of contacts between *in vitro* or patient-derived fibril and ligand, and average binding free energies (kcal mol^{-1}) for Congo red binding to either the equilibrated *in vitro* or the equilibrated patient-derived fibril structure. The standard deviation given in the parentheses is calculated over two independent trajectories.

$\text{A}\beta$ fibril	Position/orientation	RMSD (\AA)	Contacts	ΔG_{GBSA}
<i>In vitro</i>	<i>In vitro</i> , PL	1.67 (0.73)	377 (10)	-30.0 (4.0)
<i>In vitro</i>	<i>In vitro</i> , PR	1.62 (1.07)	385 (12)	-33.3 (5.9)
Patient-derived	$PD_{autodock}$, PL ^a	0.95 (0.27)	641 (32)	-45.9 (5.2)
Patient-derived	$PD_{molegro}$, PR ^a	1.12 (0.27)	409 (29)	-38.8 (6.8)

^aPL = parallel and PR = perpendicular to the fibril axis.

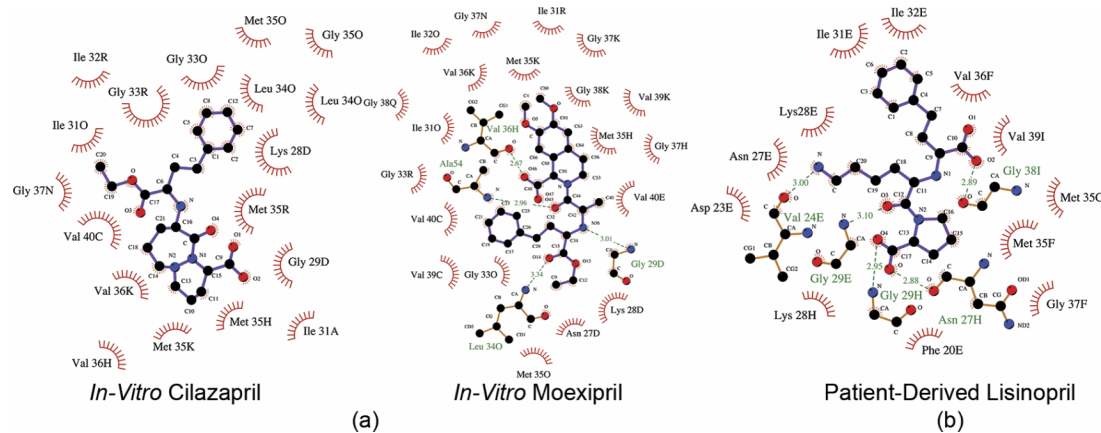


FIG. 8. Hydrophobic interactions (a) between various residues of *in vitro* fibril-cilazapril/moexipril (b) patient-derived fibril-lisinopril. The strands A-F belongs to β -sheet 1, strands G-L belongs to β -sheet 2, and strands M-R belongs to β -sheet 3.

of the central column or the three β -sheets. This argument is consistent with the number of contacts listed in Table V where we see that all ACE inhibitors except captopril and trandolapril form an equal or larger number of contacts with the *in vitro* structure than Congo red forms. The binding energies the ten ACE inhibitors bound to the equilibrated patient-derived fibril have a larger spread than seen when binding to the *in vitro* structures, and it is difficult to see a clear pattern. However, we see that with the exception of lisinopril the ACE inhibitors form only about half the number of contacts than Congo red when binding to the patient-derived structure.

In order to compare the binding affinities for the two fibrils, we focus in our further discussion only on the binding poses with the lowest binding free energies and list these again in Table VI. We compare the free energies of these binding poses with the corresponding lowest-free energy binding poses found for Congo red by calculating $\Delta\Delta G_{GBSA} = \Delta G_{\text{pril}} - \Delta G_{\text{Congo Red}}$, i.e., the difference between the selected lowest binding free energies for all *in vitro*/patient-derived fibril-ACE inhibitor complexes and the corresponding *in vitro*/patient-derived fibril-Congo red complexes, and present this quantity in Figure 9. This graph shows that the binding free energies of all ACE inhibitors except captopril are lower than the ones for Congo red when these ligands bind to the *in vitro* fibril model. Hence, no matter where they bind, i.e., to a specific strand(s) or to the central column, the majority of the ACE inhibitors bind better than Congo red to the *in vitro* A β

fibril structure. On the other hand, none of the angiotensin converting enzyme inhibitors shows favorable interactions with the patient-derived fibril structure as their ΔG_{GBSA} values are higher than the ones found for the patient-derived fibril-Congo red system. Only lisinopril has binding free energies that are within the error bars comparable the Congo red values; i.e., only lisinopril exhibit a similar binding affinity as that of Congo red to the patient-derived fibril structure. The close binding energies result from their similar binding patterns. As does Congo red, lisinopril interacts only with residues located on β -sheet 2 of the patient-derived fibril and is tightly bound there between two strands. Most unfavorable are the binding energies of benazepril and captopril. These two ligands miss the interaction with the residues on various strands of the three β -sheets. Instead, they interact with loop regions in the three β -sheets of the patient-derived fibril. The higher fluctuation of these residues leads to looser binding of the two ligands. We note, however, that Li and Ngo have reported a similar binding pose as the one observed for these two ligands when docking curcumin, naproxen, and ibuprofen to the three-layer or six-layer *in vitro* fibril structure.³⁷

Throughout the 300 ns of the simulation that led to structure of the equilibrated equilibrium *in vitro* fibril model, the shape and structure of the central column were maintained and the structure stayed close to the start configuration. However, the central column is lost for the equilibrium patient-derived fibril model, which may impact the stability

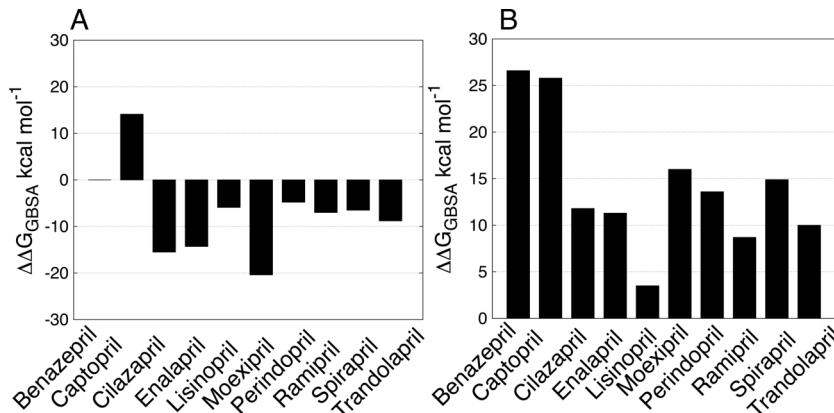


FIG. 9. Difference between the lowest binding free energies of ACE inhibitors bound to either *in vitro* or patient-derived A β structure and the energies of the corresponding fibril-Congo red systems. Values are given in kcal mol $^{-1}$ ($\Delta\Delta G_{GBSA}$) and calculated using the last 10 ns of the respective trajectories. For each fibril-ligand system, we have selected from the binding site generated by Autodock Vina or Molegro the one with lower energy. The figure on the left-hand side is for the *in vitro* fibril-ligand system and on the right is for the patient-derived fibril-ligand system.

TABLE III. List of *in vitro*/patient-derived fibril residues displaying hydrogen bond interaction with various ACE inhibitors for the lowest binding free energies systems.

Ligand	<i>In vitro</i>	Patient-derived
Benazepril	Gly25, Ser26, Gly38	Gly25 and Asn27
Captopril	Gly38, Gly37	Phe20, Glu22, Lys28
Cilazapril		His14, Val12, Asn27
Enalapril	Val39, Gly29, Val39	Val24, Gly29, Glu22
Lisinopril	Gly29, Phe19, Phe20, Asp23	Gly38, Val24, Asn27, Gly29
Moexipril	Leu34, Ala30, Val36, Gly29	Ser26, Asn27
Perindopril	Gly38, Leu34, Val40	Gly37, Gly38, Val39, Val40
Ramipril	Leu34, Gly38, Gly37	Val12, Gln15
Spirapril	Val40	Asp7
Trandolapril	Gly38	His13, Asn27

and binding patterns that fibril structure in complex with ligands. Hence, we have also considered energy minimized six-layer fibril structures derived from the first entry of the NMR ensemble of the patient-derived fibrils, and the one derived from entry #20 which is the entry with the largest root-mean-square-deviation to the first entry. All ligands (including Congo red) have been docked to both fibril models using Autodock Vina. None of the ligands bind to the central column of the fibril structure derived of entry #20, and the majority of the ligands are interacting with residues Phe19, Ala21, Glu22, Asp23, Lys28, Ile31, Ile32, Gly33, and Leu34, which are all located on various strands of β -sheet 3. However, all ligands except captopril bind to the central column of the model derived from entry #1, interacting mostly with the residues Ile32, Gly33, Leu34, Met35, and Val40 which are located on strands of β -sheet 2. Hence, unlike seen for the equilibrated structure, the ACE inhibitors bind for this NMR model to the central column in the same way as seen for the *in vitro* fibrils.

Unlike for solvation NMR, it is not clear whether the members of solid-state NMR ensemble can be interpreted as equilibrium configurations, representing a constant-temperature ensemble. This is why we have studied instead the

TABLE IV. Average binding energies (ΔG_{GBSA}) of all the ligands bound to the *in vitro* or patient-derived (PD) A β fibril structure (kcal mol $^{-1}$) calculated with MM-GBSA approach using the last 10 ns of the runs. The standard deviation given in the parentheses is calculated over two independent trajectories.

Ligand	<i>In vitro</i> A β fibril		PD A β fibril	
	<i>In vitro</i> _{autodock}	<i>In vitro</i> _{molegro}	<i>PD</i> _{autodock}	<i>PD</i> _{molegro}
Benazepril	-33.1 (12.8)	-33.3 (2.9)	-19.3 (3.0)	-16.1 (4.2)
Captopril	-19.2 (3.5)	-16.4 (5.0)	-20.1 (3.0)	-10.1 (4.5)
Cilazapril	-43.2 (6.8)	-48.8 (4.1)	-34.1 (3.5)	-17.8 (6.3)
Enalapril	-45.5 (6.0)	-47.6 (3.9)	-34.6 (5.4)	-32.0 (4.4)
Lisinopril	-39.2 (3.7)	-28.4 (5.5)	-42.4 (4.7)	-16.8 (3.9)
Moexipril	-41.3 (5.1)	-53.7 (6.5)	-29.9 (2.7)	-22.6 (4.9)
Perindopril	-38.1 (3.0)	-34.1 (5.3)	-17.1 (2.8)	-32.3 (4.8)
Ramipril	-40.3 (3.0)	-38.9 (3.5)	-37.2 (3.9)	-24.3 (3.7)
Spirapril	-31.3 (3.4)	-39.8 (3.2)	-24.5 (4.1)	-31.0 (4.2)
Trandolapril	-42.1 (3.1)	-39.5 (5.7)	-35.9 (3.2)	-28.1 (3.5)

TABLE V. Average number of contacts between ACE inhibitors and *in vitro*/patient-derived 6-layer fibril structure for the lowest binding free energies systems calculated using the last 10 ns of the sampling process. The standard deviation is given in the parenthesis.

Ligand	<i>In vitro</i>	Patient-derived
Benazepril	545 (8)	140 (20)
Captopril	170 (11)	221 (26)
Cilazapril	431 (5)	308 (27)
Enalapril	524 (8)	334 (26)
Lisinopril	327 (6)	560 (26)
Moexipril	800 (6)	428 (26)
Perindopril	363 (6)	353 (29)
Ramipril	363 (11)	308 (23)
Spirapril	449 (6)	336 (27)
Trandolapril	260 (7)	345 (23)

binding of the ACE inhibitors to equilibrated fibril structures derived from previous molecular dynamics runs of 300 ns duration. However, because the equilibrated structure differs strongly from the start structure (the NMR entry #1), and because we found different binding pattern for them in our docking study, we decided to select also the optimal binding poses of the ligands bound to this fibril, using the procedure described in the section titled Computational method. We label the so-generated systems as PD_{First} and we have simulated them in two independent molecular dynamics runs for 50 ns, using the same setup as in the previous simulations. Again, only the last 10 ns are used to approximate binding free energies by ΔG_{GBSA} values. The resulting average binding free energies of the ligands are tabulated also in Table VI.

The average binding energy of Congo red bound to the central column of the energy minimized first entry of the solid-state NMR ensemble in (PD_{First}) is much higher than the one of Congo red bound to the equilibrated patient-derived fibrils. The corresponding free energies of the ACE inhibitors are also much higher than when they bind to the equilibrated patient-derived fibrils. Hence, for the patient-derived models, Congo red and the ACE inhibitors prefer to bind to the β -sheet(s) instead the central column, the preferred binding

TABLE VI. Average lowest found binding free energies of Congo red and ten angiotensin converting enzyme inhibitors bound to either equilibrated *in vitro* A β fibril structure, equilibrated patient-derived fibril structure, or the first entry of the NMR ensemble (PD_{First}). The standard deviation given in the parentheses are calculated over two independent trajectories.

Ligand	<i>In vitro</i>	Patient-derived	PD_{First}
Congo red	-33.3 (5.9)	-45.9 (5.2)	-18.4 (3.0)
Benazepril	-33.3 (2.9)	-19.3 (3.0)	-15.7 (3.6)
Captopril	-19.2 (3.5)	-20.1 (3.0)	-4.1 (2.2)
Cilazapril	-48.8 (4.1)	-34.1 (5.4)	-14.8 (4.2)
Enalapril	-47.6 (3.9)	-34.6 (5.4)	-18.2 (3.3)
Lisinopril	-39.2 (3.7)	-42.4 (4.7)	-11.8 (3.4)
Moexipril	-53.7 (6.5)	-29.9 (2.7)	-18.2 (3.0)
Perindopril	-38.1 (3.0)	-32.3 (4.8)	-19.4 (3.1)
Ramipril	-40.3 (3.0)	-37.2 (3.9)	-13.4 (3.0)
Spirapril	-39.8 (3.2)	-31.0 (4.2)	-21.5 (2.6)
Trandolapril	-42.1 (3.1)	-35.9 (3.2)	-19.5 (2.7)

pose for the equilibrated *in vitro* fibrils. Note that the binding energies differ less between Congo red and the ACE inhibitors when bound to the energy minimized first entry of the solid-state NMR ensemble than when bound to the equilibrated patient-derived fibril.

Our guiding assumption is that binding of our components to the fibril disrupts and changes the fibril, i.e., the stronger a component binds to the fibril structure the larger is its inhibition efficiency. While the equilibrated patient-derived fibril changed over the 50 ns of our simulations by about 6 Å, and the equilibrated *in vitro* model by about 4 Å, this change is not necessarily due to binding of Congo red or the ACE Inhibitors. For instance, simulating solely the patient-derived fibril model (first entry of the NMR ensemble of 2M4J) with the same protocol as in our simulations of this fibril bound with ACE inhibitor or Congo red, the change after 50 ns is 5.4(6) Å. Bound with Congo red, the change of the fibril model is 4.9(7) Å, and bound to ACE inhibitors the change is between 4.1(3) Å (benazepril) and 5.6(2) Å (lisinopril). However, we believe that these small differences between simulations with inhibitor candidate molecules, and such without, are only due to our short simulation times. This is because the above discussed binding of the ACE inhibitors with the central column of the *in vitro* fibril (Figure 5) reduces the hydrophobic contacts between the strands of the β-sheet or across various β-sheets. The resulting lower stability of the core will over time increase the chance that the β-sheet(s) drift away from each other. Similarly, when the ACE inhibitor binds in between two β-sheets, the interaction of the ligand with the N-terminus residues will again weaken the contacts between the strands and therefore increase their flexibility and their exposure to the solvent. A similar argument can be made for the ACE inhibitors binding to the patient-derived fibril model. As shown in Figure 10, the largest probability for hydrophobic contacts is with Asn27 and Lys28. In the absence of the inhibitor, the Asn27 located on strands of one β-sheet forms contacts and a hydrogen bond with Gly9 residues located on strands of the opposite β-sheet. However, in the presence of the ligand, these contacts will be diminished or lost, reducing the contact between the two β-sheets and increasing the probability that these strands drift away from

each other. We would expect that one could see in longer simulations than accessible to us these effects on fibril stability that result from interaction of the ACE inhibitors with the two fibril models.

CONCLUSIONS

We have compared the binding of ten ACE inhibitors to *in vitro* Aβ fibril structures with their binding to patient-derived Aβ fibril structures. As a reference point, we choose the binding of Congo red to these two structures. Suitable binding poses were generated by two different docking programs (Autodock Vina and Molegro) from equilibrated structures generated in an earlier study⁶ and followed in molecular dynamics simulations. By using two docking programs, we can minimize biases associated with the choice of docking programs. For instance, in the case of Congo red, Autodock Vina predicts a parallel binding mode to both fibrils while Molegro predicts a perpendicular mode. The predicted binding sites differ significantly between the *in vitro* and patient-derived structures. The differences become most obvious when these binding energies are compared to the ones calculated for Congo red binding to the two structures. With the exception of captopril, all ACE inhibitors have a lower free energy than Congo red when binding to the *in vitro* fibril, i.e., these ligands bind tighter to the *in vitro* fibril than Congo red. However, all ACE inhibitors have *higher* binding energies than Congo red when binding to the patient-derived fibril. The majority of the ACE inhibitors interact with the residues 27–40 of the *in vitro* fibril by forming hydrophobic contacts and hydrogen bonds. The corresponding interactions with the residues of patient-derived fibril have a much broader distribution. The differences in free energies between binding to *in vitro* generated and patient-derived demonstrate the need to account for the polymorphism in Aβ fibrils when designing aggregation inhibitors. Specifically, the lower binding affinity of the ACE inhibitors to the from a medical point likely more relevant patient-derived fibrils raise doubts on the ability of these drugs to inhibit fibril formation in Alzheimer patients directly with the amyloid fibrils. It rather suggests that the protecting influence of ACE inhibitors observed in clinical studies may be due to interacting of these components with Aβ monomers or toxic oligomers and inhibiting in this way fibril formation or toxicity of aggregates. Such a scenario has been recently reported for the small molecule O₄ which by binding to Aβ fibril can enhance the formation of non-toxic matured fibrils and decreases in this way the concentration of toxic oligomers.⁷³

ACKNOWLEDGMENTS

This project was supported by the Oklahoma Center for the Advancement of Science and Technology Grant No. HR14-129 and the National Science Foundation under Grant No. CHE-1266256. The simulations were done on the BOOMER cluster of The University of Oklahoma. In addition, this work used computing resources of the Extreme Science and Engineering Discovery Environment (XSEDE),

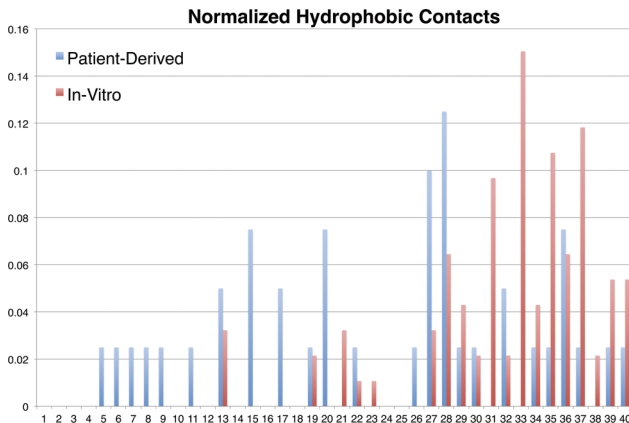


FIG. 10. Probability to form hydrophobic contacts between various residues of *in vitro* or patient-derived fibril and ACE inhibitors.

which is supported by National Science Foundation. We thank Dr. Steven R. Gwaltney at the Department of Chemistry, Mississippi State University for providing additional computer resources.

- ¹Y. Tian, B. Bassit, D. Chau, and Y.-M. Li, *Nat. Struct. Mol. Biol.* **17**(2), 151–158 (2010).
- ²S. Wood, P. H. Wen, J. Zhang, L. Zhu, Y. Luo, S. Babu-Khan, K. Chen, R. Pham, J. Esmay, T. A. Dineen, M. R. Kaller, M. M. Weiss, S. A. Hitchcock, M. Citron, W. Zhong, D. Hickman, and T. Williamson, *J. Pharmacol. Exp. Ther.* **343**(2), 460–467 (2012).
- ³A. T. Petkova, W. M. Yau, and R. Tycko, *Biochemistry* **45**(2), 498–512 (2006).
- ⁴A. K. Paravastu, R. D. Leapman, W. M. Yau, and R. Tycko, *Proc. Natl. Acad. Sci. U. S. A.* **105**(47), 18349–18354 (2008).
- ⁵J. X. Lu, W. Qiang, W. M. Yau, C. D. Schwieters, S. C. Meredith, and R. Tycko, *Cell* **154**(6), 1257–1268 (2013).
- ⁶E. J. Alred, M. Phillips, W. M. Berhanu, and U. H. E. Hansmann, *Protein Sci.* **24**(6), 923–935 (2015).
- ⁷W. M. Berhanu, F. Yaşar, and U. H. E. Hansmann, *ACS Chem. Neurosci.* **4**(11), 1488–1500 (2013).
- ⁸E. J. Alred, E. G. Scheele, W. M. Berhanu, and U. H. E. Hansmann, *J. Chem. Phys.* **141**(17), 175101 (2014).
- ⁹Q. Wang, X. Yu, L. Li, and J. Zheng, *Curr. Pharm. Des.* **20**(8), 1223–1243 (2014).
- ¹⁰F. Re, C. Airoldi, C. Zona, M. Masserini, B. La Ferla, N. Quattrochi, and F. Nicotra, *Curr. Med. Chem.* **17**(27), 2990–3006 (2010).
- ¹¹S. Fuse, K. Matsumura, Y. Fujita, H. Sugimoto, and T. Takahashi, *Eur. J. Med. Chem.* **85**, 228–234 (2014).
- ¹²K. G. Yiannopoulou and S. G. Papageorgiou, *Ther. Adv. Neurol. Disord.* **6**(1), 19–33 (2013).
- ¹³J. Nasica-Labouze, P. H. Nguyen, F. Sterpone, O. Berthoumieu, N.-V. Buchete, S. Coté, A. De Simone, A. J. Doig, P. Faller, A. Garcia, A. Laio, M. S. Li, S. Melchionna, N. Mousseau, Y. Mu, A. Paravastu, S. Pasquali, D. J. Rosenman, B. Strodel, B. Tarus, J. H. Viles, T. Zhang, C. Wang, and P. Derreumaux, *Chem. Rev.* **115**(9), 3518–3563 (2015).
- ¹⁴M. W. Riepe, G. Adler, B. Ibach, B. Weinkauf, I. Gunay, and F. Tracik, *J. Clin. Psychiatry* **8**(5), 258–263 (2006).
- ¹⁵N. D. Parikh and D. K. Klimov, *J. Phys. Chem. B* **119**(35), 11568–11580 (2015).
- ¹⁶C. Lockhart and D. K. Klimov, *Biophys. J.* **103**(11), 2341–2351 (2012).
- ¹⁷Y. Porat, A. Abramowitz, and E. Gazit, *Chem. Biol. Drug Des.* **67**(1), 27–37 (2006).
- ¹⁸K. Abe, M. Kato, and H. Saito, *Neurosci. Res.* **29**(2), 129–134 (1997).
- ¹⁹C. Wu, M. T. Bowers, and J.-E. Shea, *Biophys. J.* **100**(5), 1316–1324 (2011).
- ²⁰M. Necula, R. Kayed, S. Milton, and C. G. Glabe, *J. Biol. Chem.* **282**(14), 10311–10324 (2007).
- ²¹H. C. Huang, K. Xu, and Z. F. Jiang, *J. Alzheimer's Dis.* **32**(4), 981–996 (2012).
- ²²F. Yang, G. P. Lim, A. N. Begum, O. J. Ubeda, M. R. Simmons, S. S. Ambegaokar, P. P. Chen, R. Kayed, C. G. Glabe, S. A. Frautschy, and G. M. Cole, *J. Biol. Chem.* **280**(7), 5892–5901 (2005).
- ²³Y. Feng, X. P. Wang, S. G. Yang, Y. J. Wang, X. Zhang, X. T. Du, X. X. Sun, M. Zhao, L. Huang, and R. T. Liu, *Neurotoxicology* **30**(6), 986–995 (2009).
- ²⁴T. Richard, P. Poupart, M. Nassra, Y. Papastamoulis, M.-L. Iglesias, S. Krisa, P. Waffo-Teguo, J.-M. Mérillon, and J.-P. Monti, *Bioorg. Med. Chem.* **19**(10), 3152–3155 (2011).
- ²⁵D. E. Ehrnhoefer, J. Bieschke, A. Boeddrich, M. Herbst, L. Masino, R. Lurz, S. Engemann, A. Pastore, and E. E. Wanker, *Nat. Struct. Mol. Biol.* **15**(6), 558–566 (2008).
- ²⁶L. O. Tjernberg, J. Näslund, F. Lindqvist, J. Johansson, A. R. Karlström, J. Thyberg, L. Terenius, and C. Nordstedt, *J. Biol. Chem.* **271**(15), 8545–8548 (1996).
- ²⁷Q. Nie, X.-g. Du, and M.-y. Geng, *Acta Pharmacol. Sin.* **32**(5), 545–551 (2011).
- ²⁸P. Pratim Bose, U. Chatterjee, C. Nerelius, T. Govender, T. Norström, A. Gogoll, A. Sandegren, E. Göthelid, J. Johansson, and P. I. Arvidsson, *J. Med. Chem.* **52**(24), 8002–8009 (2009).
- ²⁹N. M. Davies, P. G. Kehoe, Y. Ben-Shlomo, and R. M. Martin, *J. Alzheimer's Dis.* **26**(4), 699–708 (2011).
- ³⁰I. Hajjar, L. Brown, W. J. Mack, and H. Chui, *Arch. Neurol.* **69**(12), 1632–1638 (2012).
- ³¹L. Ferrington, L. E. Palmer, S. Love, K. J. Horsburgh, P. A. T. Kelly, and P. G. Kehoe, *Am. J. Transl. Res.* **4**(2), 151–164 (2012).
- ³²N. J. Brown and D. E. Vaughan, *Circulation* **97**(14), 1411–1420 (1998).
- ³³W. Q. Qiu, M. Mwamburi, L. M. Besser, H. Zhu, H. Li, M. Wallack, L. Phillips, L. Qiao, A. E. Budson, R. Stern, and N. Kowall, *J. Alzheimer's Dis.* **37**(2), 421–428 (2013).
- ³⁴W. W. Qiu, A. Lai, T. Mon, M. Mwamburi, W. Taylor, J. Rosenzweig, N. Kowall, R. Stern, H. Zhu, and D. C. Steffens, *Am. J. Geriatric Psychiatry* **22**(2), 177–185 (2014).
- ³⁵K. M. Sink, X. Leng, J. Williamson, S. B. Kritchevsky, K. Yaffe, L. Kuller, S. Yasuf, H. Atkinson, M. Robbins, B. Psaty, and D. C. Goff, *Arch. Intern. Med.* **169**(13), 1195–1202 (2009).
- ³⁶C. Wu, J. Scott, and J.-E. Shea, *Biophys. J.* **103**(3), 550–557 (2012).
- ³⁷S. T. Ngo and M. S. Li, *J. Phys. Chem. B* **116**(34), 10165–10175 (2012).
- ³⁸M. H. Viet, S. T. Ngo, N. S. Lam, and M. S. Li, *J. Phys. Chem. B* **115**(22), 7433–7446 (2011).
- ³⁹C. N. Cavasotto and A. J. Orry, *Curr. Top. Med. Chem.* **7**(10), 1006–1014 (2007).
- ⁴⁰C. M. Venkatachalam, X. Jiang, T. Oldfield, and M. Waldman, *J. Mol. Graphics Modell.* **21**(4), 289–307 (2003).
- ⁴¹G. M. Morris, D. S. Goodsell, R. S. Halliday, R. Huey, W. E. Hart, R. K. Belew, and A. J. Olson, *J. Comput. Chem.* **19**(14), 1639–1662 (1998).
- ⁴²G. Rastelli, A. Del Rio, G. Degliesposti, and M. Sgobba, *J. Comput. Chem.* **31**(4), 797–810 (2010).
- ⁴³B. Wang, L. Li, T. D. Hurley, and S. O. Meroueh, *J. Chem. Inf. Model.* **53**(10), 2659–2670 (2013).
- ⁴⁴W. M. Berhanu and U. H. E. Hansmann, *Adv. Protein Chem. Struct. Biol.* **96**, 113–141 (2014).
- ⁴⁵W. M. Berhanu and U. H. E. Hansmann, *Proteins: Struct., Funct., Bioinf.* **81**(9), 1542–1555 (2013).
- ⁴⁶Y. Shao, L. F. Molnar, Y. Jung, J. Kussmann, C. Ochsenfeld, S. T. Brown, A. T. B. Gilbert, L. V. Slipchenko, S. V. Levchenko, D. P. O'Neill, R. A. Distasio, Jr., R. C. Lochan, T. Wang, G. J. O. Beran, N. A. Besley, J. M. Herbert, C. Yeh Lin, T. Van Voorhis, S. Hung Chien, A. Sodt, R. P. Steele, V. A. Rassolov, P. E. Maslen, P. P. Korambath, R. D. Adamson, B. Austin, J. Baker, E. F. C. Byrd, H. Dachsel, R. J. Doerksen, A. Dreuw, B. D. Dunietz, A. D. Dutoi, T. R. Furlani, S. R. Gwaltney, A. Heyden, S. Hirata, C.-P. Hsu, G. Kedziora, R. Z. Khallilin, P. Klunzinger, A. M. Lee, M. S. Lee, W. Liang, I. Lotan, N. Nair, B. Peters, E. I. Proynov, P. A. Pieniazek, Y. Min Rhee, J. Ritchie, E. Rosta, C. David Sherrill, A. C. Simonett, J. E. Subotnik, H. Lee Woodcock III, W. Zhang, A. T. Bell, A. K. Chakraborty, D. M. Chipman, F. J. Keil, A. Warshel, W. J. Hehre, H. F. Schaefer III, J. Kong, A. I. Krylov, P. M. W. Gill, and M. Head-Gordon, *Phys. Chem. Chem. Phys.* **8**(27), 3172–3191 (2006).
- ⁴⁷T. A. Halgren, *J. Comput. Chem.* **17**(5–6), 490–519 (1996).
- ⁴⁸F. Y. Dupradeau, A. Pigache, T. Zaffran, C. Savineau, R. Lelong, N. Grivel, D. Lelong, W. Rosanski, and P. Cieplak, *Phys. Chem. Chem. Phys.* **12**(28), 7821–7839 (2010).
- ⁴⁹O. Trott and A. J. Olson, *J. Comput. Chem.* **31**(2), 455–461 (2010).
- ⁵⁰R. Thomsen and M. H. Christensen, *J. Med. Chem.* **49**(11), 3315–3321 (2006).
- ⁵¹W. Humphrey, A. Dalke, and K. Schulter, *J. Mol. Graphics* **14**(1), 33–38 (1996).
- ⁵²J. E. Chambers, H. W. Chambers, E. C. Meek, K. E. Funck, M. Bhavaraju, S. R. Gwaltney, and R. B. Pringle, *Toxicol. Sci.* **143**(1), 46–53 (2014).
- ⁵³A. D. MacKerell, D. Bashford, M. Bellott, R. L. Dunbrack, J. D. Evanseck, M. J. Field, S. Fischer, J. Gao, H. Guo, S. Ha, D. Joseph-McCarthy, L. Kuchnir, K. Kuczera, F. T. K. Lau, C. Mattos, S. Michnick, T. Ngo, D. T. Nguyen, B. Prodhom, W. E. Reiher, B. Roux, M. Schlenkrich, J. C. Smith, R. Stote, J. Straub, M. Watanabe, J. Wiorkiewicz-Kuczera, D. Yin, and M. Karplus, *J. Phys. Chem. B* **102**(18), 3586–3616 (1998).
- ⁵⁴A. D. MacKerell, M. Feig, and C. L. Brooks III, *J. Comput. Chem.* **25**(11), 1400–1415 (2004).
- ⁵⁵D. A. Case, T. A. Darden, T. E. Cheatham, C. L. Simmerling, J. Wang, R. E. Duke, R. Luo, R. C. Walker, W. Zhang, K. M. Merz, B. Roberts, S. Hayik, A. Roitberg, G. Seabra, J. Swails, A. W. Goetz, I. Kolossváry, K. F. Wong, F. Paesani, J. Vanicek, R. M. Wolf, J. Liu, X. Wu, S. R. Brozell, T. Steinbrecher, H. Gohlke, Q. Cai, X. Ye, J. Wang, M. J. Hsieh, G. Cui, D. R. Roe, D. H. Mathews, M. G. Seston, R. Salomon-Ferrer, C. Sagué, V. Babin, T. Luchko, S. Gusarov, A. Kovalenko, and P. A. Kollman, (University of California, San Francisco, 2012).
- ⁵⁶V. Hornak, R. Abel, A. Okur, B. Strockbine, A. Roitberg, and C. Simmerling, *Proteins* **65**(3), 712–725 (2006).
- ⁵⁷J. Wang, R. M. Wolf, J. W. Caldwell, P. A. Kollman, and D. A. Case, *J. Comput. Chem.* **25**(9), 1157–1174 (2004).
- ⁵⁸W. L. Jorgenson, J. Chandrasekhar, J. D. Madura, R. W. Impey, and M. L. Klein, *J. Chem. Phys.* **79**(2), 926–935 (1983).

- ⁵⁹U. Essmann, L. Perera, M. L. Berkowitz, T. Darden, H. Lee, and L. G. Pedersen, *J. Chem. Phys.* **103**(19), 8577–8593 (1995).
- ⁶⁰T. Darden, D. York, and L. Pedersen, *J. Chem. Phys.* **98**(12), 10089–10092 (1993).
- ⁶¹S. Miyamoto and P. A. Kollman, *J. Comput. Chem.* **13**(8), 952–962 (1992).
- ⁶²S. E. Feller, Y. Zhang, R. W. Pastor, and B. R. Brooks, *J. Chem. Phys.* **103**, 4613–4621 (1995).
- ⁶³H. Sun, Y. Li, S. Tian, L. Xu, and T. Hou, *Phys. Chem. Chem. Phys.* **16**(31), 16719–16729 (2014).
- ⁶⁴L. Xu, H. Sun, Y. Li, J. Wang, and T. Hou, *J. Phys. Chem. B* **117**(28), 8408–8421 (2013).
- ⁶⁵J. Ma, *Structure* **13**(3), 373–380 (2005).
- ⁶⁶T. Hou, J. Wang, Y. Li, and W. Wang, *J. Chem. Inf. Model.* **51**(1), 69–82 (2011).
- ⁶⁷N. Homeyer and H. Gohlke, *Mol. Inf.* **31**(2), 114–122 (2012).
- ⁶⁸J. Wang, P. Morin, W. Wang, and P. A. Kollman, *J. Am. Chem. Soc.* **123**(22), 5221–5230 (2001).
- ⁶⁹J. Park, B. Kahng, and W. Hwang, *PLoS Comput. Biol.* **5**(9), e10000492 (2009).
- ⁷⁰L. Zheng and W. Yang, *J. Chem. Theory Comput.* **8**(3), 810–823 (2012).
- ⁷¹T. Miura, C. Yamamiya, M. Sasaki, K. Suzuki, and H. Takeuchi, *J. Raman Spectrosc.* **33**(7), 530–535 (2002).
- ⁷²A. K. Schütz, A. Soragni, S. Hornemann, A. Aguzzi, M. Ernst, A. Böckmann, and B. H. Meier, *Angew. Chem., Int. Ed.* **50**(26), 5956–5960 (2011).
- ⁷³J. Bieschke, M. Herbst, T. Wiglenda, R. P. Friedrich, A. Boeddrich, F. Schiele, D. Kleckers, J. M. Lopez del Amo, B. A. Grüning, Q. Wang, M. R. Schmidt, R. Lurz, R. Anwyl, S. Schnoegl, M. Fändrich, R. F. Frank, B. Reif, S. Günther, D. M. Walsh, and E. E. Wanker, *Nat. Chem. Biol.* **8**(1), 93–101 (2012).